

## Supplementary Information: Complex Magnetic Orders in Small Cobalt-Benzene Molecules

J. W. González,<sup>1,2,\*</sup> T. Alonso-Lanza,<sup>1,2</sup> F. Delgado,<sup>2,3,4</sup> F. Aguilera-Granja,<sup>2,5</sup> A. Ayuela.<sup>1,2</sup>

<sup>(1)</sup> *Centro de Física de Materiales (CFM-MPC) Centro Mixto CSIC-UPV/EHU,  
Manuel de Lardizabal 5, E-20018 Donostia-San Sebastián, Spain.*

<sup>(2)</sup> *Donostia International Physics Center (DIPC),  
Manuel de Lardizabal 4, E-20018 San Sebastián, Spain*

<sup>(3)</sup> *IKERBASQUE, Basque Foundation for Science, E-48013 Bilbao, Spain.*

<sup>(4)</sup> *Departamento de Física, Universidad de La Laguna, La Laguna E-38204, Tenerife, Spain.*

<sup>(5)</sup> *Instituto de Física, Universidad Autónoma de San Luis Potosí, 78000 San Luis Potosí, México.*

(Dated: May 11, 2017)

### SI. DFT DETAILS

#### A. LCAO methods: SIESTA

SIESTA calculations were performed using the exchange and correlation potentials with the generalized gradient approximation (GGA) in Perdew-Burke-Ernzerhof form.<sup>1</sup> We used an electronic temperature of 25 meV and a mesh cutoff of 250 Ry for all the calculations. The atomic cores were described using nonlocal norm-conserving relativistic Troullier-Martins<sup>2</sup> pseudopotentials with non-linear core corrections factorized in the Kleyman-Bylander form. The pseudopotentials were tested to ensure that they accurately reproduce the eigenvalues of different excited states of a bare atom. We tested the cobalt pseudopotential against the bulk cobalt. We use the  $4s^1 3d^8$  valence configuration, and found that the ground state was the hcp structure, which had a stability of 0.025 eV/atom greater than that of the fcc structure. For the hcp structure, the first neighbor distance was 2.54 Å and the magnetic moment per atom was 1.64  $\mu_B$ , in good agreement with experimental results.<sup>3</sup> The cobalt pseudopotential was described in detail and used to study  $\text{Co}_{13}$  clusters adsorbed onto graphene in a previous study.<sup>4</sup> The basis sets for cobalt, hydrogen, and carbon were the double-polarized basis sets identified in previous studies.

Geometric relaxations used conjugate gradient structure optimization. The hydrogen atoms of the benzene rings made it necessary to impose small convergence thresholds on forces of the order of  $10^{-3}$  Ry/bohr  $\approx 2.57 \times 10^{-3}$  eV/Å. We found that imposing less strict convergence conditions over both the energies and the forces may erroneously lead to deformed structures. In each case, a single  $\Gamma$ -point was chosen for the calculations and 15 Å of empty space was added to avoid interactions between nearest-neighbors cells.

#### B. Plane-waves methods: Quantum ESPRESSO and VASP

Plane-wave methods such as QUANTUM ESPRESSO<sup>5</sup> and VASP<sup>6,7</sup> were used. Self-consistent calculations were performed very accurately using a plane-wave kinetic energy cutoff of 80 Ry. As in the SIESTA calculations, the generalized gradient approximation in exchange-correlation was in Perdew-Burke-Ernzerhof (PBE)<sup>1</sup> form. Norm-conserving Troullier-Martins pseudopotentials<sup>2</sup> were used in Quantum ESPRESSO, and a projector augmented wave potential construction was used in VASP. All the atoms were allowed to relax by conjugate gradients until the forces converged, with a tolerance of  $10^{-4}$  eV/Å. We then checked that the relaxed geometries reproduced the SIESTA results.

#### C. Full potential methods: ELK

An all-electron full-potential linearised augmented-plane wave (FP-LAPW) were performed using the ELK code. The electronic exchange-correlation potential was treated within the local spin density approximation (LSDA)<sup>8</sup> to avoid gradients effects of the generalized gradient approximation in the non-collinear calculations. Wavefunctions in the interstitial density and potential were expanded into plane waves with a wavevector cutoff of  $k_{max} = 15/R_{Co}$ , where  $R_{Co} \approx 1.16$  Å is the muffin-tin radius of cobalt.

#### D. Geometry

The Cartesian coordinates of the  $\text{Co}_3\text{Bz}_3$  optimized structure shown in Figure 1 of the main text are presented in table S1.

\*Corresponding author: sgkgosaj@ehu.eus

TABLE S1: Cartesian coordinates (in Å) of the Co<sub>3</sub>Bz<sub>3</sub> optimized structure.

Co	0.00000	0.00000	0.00000
Co	12.98486	1.19078	14.99998
Co	12.98452	13.81123	14.99992
C	1.55469	14.99907	1.44195
C	1.54217	1.24169	0.72072
C	1.54216	1.24161	14.27903
C	1.55466	14.99890	13.55797
C	1.54196	13.75634	14.27919
C	1.54197	13.75643	0.72086
C	12.15778	2.52712	1.44058
C	11.11924	1.83880	0.72069
C	11.11931	1.83880	14.27908
C	12.15772	2.52700	13.55916
C	13.21217	3.18377	14.28029
C	13.21210	3.18376	0.71938
C	12.15760	12.47503	1.44053
C	13.21213	11.81836	0.71930
C	13.21203	11.81847	14.28020
C	12.15772	12.47507	13.55908
C	11.11912	13.16336	14.27900
C	11.11922	13.16326	0.72064
H	1.50811	14.99971	2.55134
H	1.49666	2.20399	1.27342
H	1.49662	2.20391	13.72634
H	1.50803	14.99946	12.44859
H	1.49626	12.79453	13.72609
H	1.49629	12.79467	1.27409
H	12.18057	2.49043	2.55059
H	10.33145	1.28879	1.27683
H	10.33141	1.28870	13.72304
H	12.18058	2.49030	12.44919
H	14.04625	3.66264	13.72513
H	14.04622	3.66268	1.27462
H	12.18051	12.51164	2.55054
H	14.04618	11.33955	1.27454
H	14.04626	11.33958	13.72506
H	12.18049	12.51183	12.44910
H	10.33133	13.71341	13.72299
H	10.33135	13.71333	1.27680

### SIII. SPIN HAMILTONIAN

#### A. Local spins and symmetry arguments

The DFT results indicated that the energy levels corresponding to the  $d$ -orbitals of the cobalt atoms in a CoBz cluster split in two, with the lowest orbital triplet almost fully occupied and a half-occupied excited doublet. Thus, the filling of the levels following the Hund's rule leads to a spin  $S = 3/2$ . Although the degeneracy of the lowest orbital triplet is partially broken due to the new crystal field in the Co<sub>3</sub>Bz<sub>3</sub> cluster, the qualitative filling is essentially conserved. Consequently, we assumed later that each cobalt behaves as a  $S = 3/2$  spin. This spin is also compatible with the <sup>4</sup>F ground state observed in the gas phase.<sup>9</sup>

In order to include the local magnetic anisotropy,

we made the following symmetry considerations. An isolated CoBz unit has  $C_{6v}$  symmetry. The local spin Hamiltonian compatible with this symmetry can be written in terms of the (tesseral tensor) Stevens operators  $\hat{O}_k^q(S)$  as<sup>10</sup>

$$H_i = \sum_{k=2,4,6} \sum_{q=-k}^k B_k^q \hat{O}_k^q(S_i), \quad (S1)$$

where  $B_k^q$  are real coefficients.  $\hat{O}_k^q(S)$  are in turn linear combinations of spin operator components. The lowest order non-isotropic term corresponds to the operator  $\hat{O}_2^0 \propto (S_i^{z_i})^2$ , which is the uniaxial term used in this work. Higher (even) powers of  $S_i^{z_i}$  do not introduce any qualitative change to the energy spectrum and they can be thought as a renormalized  $D$ -value, hence we neglected them. All these terms commute with  $S_i^{z_i}$ , and thus, they do not introduce mixing between the eigenstates of  $S_i^{z_i}$ . Importantly, the lowest transverse terms compatible with the  $C_{6v}$  symmetry of CoBz involves the sixth power of the ladder operator,  $(S_i^\pm)^6$ . They therefore do not contribute to the spectrum of a spin  $S \leq 5/2$ , so we discarded them.

#### B. Spin Hamiltonian parameters

As stated in the main text, the spin Hamiltonian Eq. (1) contains three fitting parameters,  $J$ ,  $J'$  and  $D$ , for a given local spin  $S$ . Herein, we described in detail the derivation of the optimal parameters that best match the information provided by the DFT calculations.

The electronic structure calculations of a single CoBz molecule gave an energy difference of 8.2 meV between configurations with the magnetization out of plane (lowest energy) and in-plane, suggesting that the easy axis would be out of plane with  $D \approx -4.1$  meV for  $S = 3/2$ . The DFT results for the CoBz complex show that changing the magnetization orientation along the benzene plane did not significantly change the energy of the complex, in good agreement with our symmetry arguments. We found that the benzene rings are not deformed appreciably when a Co<sub>3</sub>Bz<sub>3</sub> cluster is formed, so it may be tempting to use the local anisotropy of each CoBz unit. However, this option was strongly discouraged by the DFT results. First, the distances between the cobalt atoms (2.34 Å) were of the same order than the distance between a cobalt atom and the closest carbon, approximately 2 Å. Second, the charge of the cobalt ions in a CoBz and the Co<sub>3</sub>Bz<sub>3</sub> cluster differ by half an electron. Third, the distances between cobalt atoms and the closest benzene plane changes by as much as 9%.

The most important characteristics to reproduce from the DFT results, shown in Fig. (2)

- a ground state with magnetization in the cobalt atom plane,

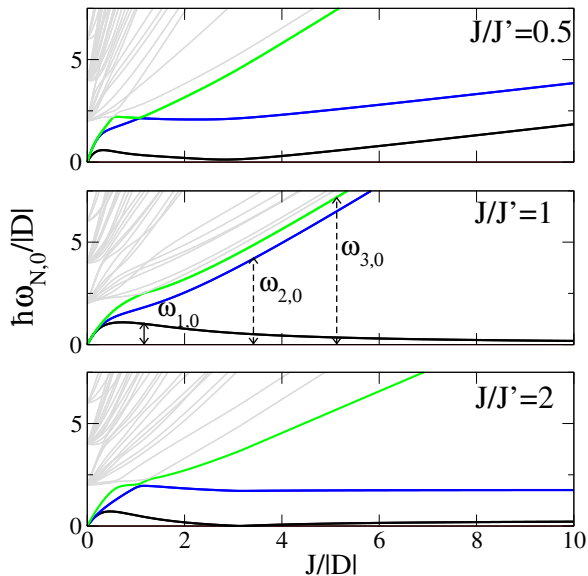


FIG. S1: (Color online) Excitation energies from the ground state vs.  $J/|D|$  for three different  $J/J'$  ratios.  $\hbar\omega_{1,0}$  (black line) is identified with the 0.25 meV non-collinear excitation in Fig. (2)  $\hbar\omega_{2,0}$  (blue line) with the 22 meV excitation, and  $\hbar\omega_{3,0}$  (green line) with the antiferromagnetic configuration at 72 meV.

- a first excitation at  $\Delta_1 \sim 0.2$  meV, with in-plane magnetization,
- a second excitation at  $\Delta_2 \sim 22$  meV (in-plane magnetization), and
- a third excitation at  $\Delta_3 \sim 72$  meV with out-of-plane magnetization.

Our approach to set the three parameters consisted of the following steps. First, for three different  $J/J'$  scenarios, we looked at the qualitative behavior of the energy spectra with the  $J/|D|$  ratio between the limits of the isolated CoBz units ( $J/|D| = 0$ ), and the isotropic cluster ( $J \gg |D|$ ). Crucially, the magnetic configurations resulting from the non-collinear calculations indicated the dominance of spin-exchange interactions over anisotropy, so the most natural scenario corresponded to  $J \gtrsim |D|$ . The excitation energies  $\hbar\omega_{N,0}$  from the ground state are plotted against  $J/|D|$  for three different  $J/J'$  values in Fig. S1. We associated the first excitation with the DFT electronic state at 0.2 meV above the ground state. The second energy level was ascribed to the configurations found 22.2 meV above the ground state. Thus, we choose the parameters such that  $\omega_{1,0}/\omega_{2,0} = \Delta_1/\Delta_2 \approx 0.01$  while keeping the gap  $\hbar\omega_{2,0}$  as large as possible in terms of  $D$  to avoid unrealistically large anisotropy barriers. The third magnetic configuration at 72 meV, identified from the DFT results as an AFM configuration with out-of-plane magnetization, was taken as the third excited state of the

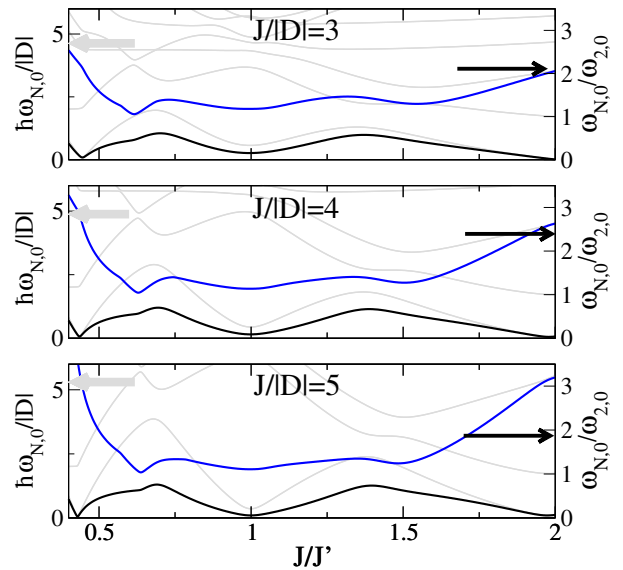


FIG. S2: (Color online) Excitation energies (gray lines, left axis) from the ground state vs. the ratio  $J/J'$  for three different ratios  $J/|D|$ . The ratios  $\omega_{1,0}/\omega_{2,0}$  and  $\omega_{3,0}/\omega_{2,0}$  (right axis) are plotted as thick blue and black lines respectively. These ratios approach the DFT results of Fig. 2 when  $J/J' = 2$  for  $J/|D| = 5$ .

model. Comparing the energy spectra shown in Fig. (2) and Fig. S1, we observe that the first two conditions are quantitatively satisfied for  $J/|D| \approx 2.5$  in the asymmetric case with  $J/J' \approx 0.5$  or for  $J/|D| \in [2.5, 6]$  with  $J/J' = 2$ . The symmetric configuration  $J = J'$  did not provide a qualitative agreement for any  $J/|D|$  ratio.

A more quantitative picture is obtained by inspection of the excitation spectrum versus  $J/J'$ , shown in Fig. S2. The  $\omega_{1,0}/\omega_{2,0}$  and  $\omega_{3,0}/\omega_{2,0}$  ratios were plotted versus  $J/J'$  for three different values of  $J/|D|$ , with the ideal ratios close to 0 and 3.3, respectively. For reference, the corresponding excitation spectra are plotted in grey. The best agreement is found for  $J/J' \approx 0.47$  and, especially, for  $J/J' \approx 2$ . Again, the symmetric case ( $J = J'$ ) was far from the ideal ratios for any  $J/|D|$  in the considered range of parameters.

Summing up, optimal agreement with the DFT results was found for  $(D, J, J') = (-12.64, 63.2, 31.6)$  meV and  $(D, J, J') = (-12.64, 63.2, 134)$  meV. These values are higher than those typically found within SMMs. However, the cobalt centers in the  $\text{Co}_3\text{Bz}_3$  cluster are much closer, so a direct exchange mechanism is possible. Thus, it seems clear that both local magnetic anisotropy due to the benzene rings and the direct-exchange between the local moments associated to the Co atoms plays a crucial role.

### C. Connection to experiments

Before trying to connect to an specific measurement, it is worth looking at the energy scales involved. If we denoted the excitation energies from the ground state to the first and second excited states as  $\hbar\omega_{1,0}$  and  $\hbar\omega_{2,0}$  respectively, and introducing the temperature  $T_M = \hbar\omega_{M,0}/k_B$ , magnetic field  $B_M = \hbar\omega_{M,0}/(g\mu_B)$ , and frequency  $f_M = 2\pi\omega_{M,0}$ , we got the following energy scales at zero external field:  $\hbar\omega_{1,0} \sim 0.2$  meV ( $T_1 \sim 2$  K,  $B_1 \sim 2$  T, and  $f_1 \sim 50$  GHz), and  $\hbar\omega_{2,0} \sim 22$  meV ( $T_2 \sim 250$  K,  $B_2 \sim 190$  T, and  $f_2 \sim 5$  THz). This had the following consequences for the possible experimental observation. Static measurements of the susceptibility may provide significant information about the lowest energy excitation for  $T \lesssim 2$  K. Furthermore, for  $T$  close to room temperature there may be other excitations not included here, like phonons. We had not found significant changes of the susceptibility with temperature or magnetic fields below 10 T. *ac* measurements of the dynamical susceptibility are also commonly used to extract additional magnetic information of SMMs, but the frequency range is limited to  $f \in [1 \text{ Hz} - 0.1 \text{ MHz}]$ ,<sup>11</sup> clearly outside the energy range of interest. High *dc*-field EPR measurements may provide an accurate spectral information. In fact, for the  $B_{dc} = 10.2$  T *J*-band, the electron spin resonance is found around 285 GHz.<sup>12</sup> For such an applied external field applied out of the Co's plane,  $\hbar\omega_{1,0} \sim 1.1$  meV and  $\hbar\omega_{2,0} \sim 1.2$  meV (275 – 286 GHz), within the range of experimental frequencies.

### D. Analysis of the EPR signal

EPR experiments apply a fixed *dc* field along a given direction, which we defined as the quantization axis  $z$ , and a small perpendicular *ac* field  $\vec{B}_{ac}(t) = \vec{B}_{ac} \sin\omega t$ , along the  $x$ -axis. For the Co-Bz molecule, the most convenient set-up corresponds to the *J*-band ( $B_{dc} = 10.2$  T) with frequencies  $2\pi\omega \approx 285$  GHz. We used time dependent perturbation theory because the perpendicular *ac* field is much smaller, with typical intensities of the order of 1 G.

The absorbed power is given as the variation of the average energy  $\langle\langle H(t) \rangle\rangle = \text{Tr}[\hat{\rho}(t)\hat{H}(t)]$  with time, where  $\hat{\rho}(t)$  is the density matrix. We here assumed a coherent dynamics. We used an interaction picture with respect to the term  $H'(t) = g\mu_b\vec{B}_{ac} \cdot \vec{S}_T \sin\omega t$  and a first order perturbative expansion for the density matrix operator. Thus, the instantaneous power was given by

$$W(t) \equiv \frac{d\langle\langle H(t) \rangle\rangle}{dt} \approx \omega\gamma B_{ac} \cos\omega t \sum_N P_N S_{N,N}^x + \frac{\omega\gamma^2 B_{ac}^2}{\hbar^2} \sum_{NM} |S_{NM}^x|^2 (P_M - P_N) \times \left[ \cos t\omega \sin t\omega_{NM} + \frac{\omega_{NM}}{\omega} (\cos t\omega_{NM} \sin t\omega - \sin 2t\omega) \right],$$

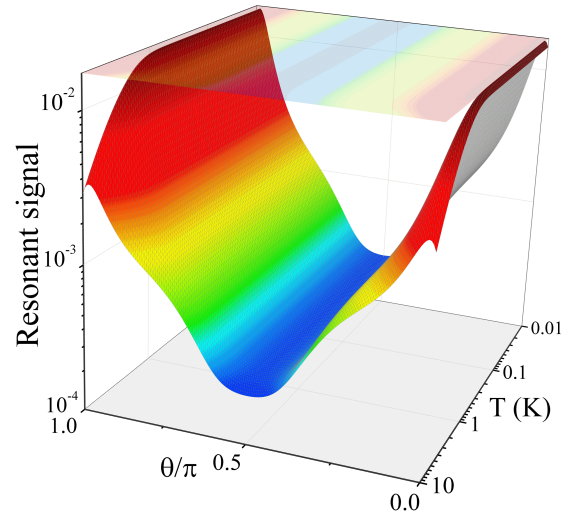


FIG. S3: (Color online) Contour plot of the on-resonant EPR signal,  $|\hat{B}_{ac} \cdot \vec{S}_{1,0}|^2(P_1 - P_0)$ , versus the angle  $\theta$  formed by the normal to the Co's plane and the *dc* magnetic field ( $\vec{B}_{ac} = \vec{B}_{ac}/|\vec{B}_{ac}|$ ). The *ac* field is parallel to one of the easy axis of atom 1 in Eq. (1).

$$(S2)$$

where  $S_{NM}^x = \sum_l \langle N | S_l^x | M \rangle$ ,  $\gamma = g\mu_B$  is the gyromagnetic ratio, and  $P_M$  denotes the thermal equilibrium occupation of the energy level  $M$ .

There are however two considerations to be made in order to connect the absorbed power  $W(t)$  with the EPR signal. First, the absorption signal of the EPR measurement corresponds to the average of instantaneous power over a measurement time  $\tau \gg 2\pi/\omega$ . Second, the coupling of the spin system with the environment induces a dissipative dynamics. When two energy levels are close to resonance for a given frequency  $\omega$ , i.e.,  $|\omega - \omega_{NM}|/\omega \ll 1$ , the incoherent dynamics introduces two new time scales, the *longitudinal or relaxation time*  $T_1$  and the *transversal or decoherence time*  $T_2$ .<sup>10</sup> These two time scales determine the line-shape of the EPR absorption spectra and, in particular, the width of the resonances, given essentially by  $T_2^{-1}$ .

When  $W(t)$  is averaged over a long period of time  $\tau \gg 1/\omega$ , the first term cancels. For a frequency window  $|\omega - \omega_{NM}|T_2 \ll 1$ , the *steady-state* absorbed power is then proportional to  $\gamma^2 B_{ac}^2 |S_{NM}^x|^2 (P_N - P_M)$ . The incoherent dynamics modifies the time dependence in the last part of Eq. (S2) which, in the frequency domain, leads to a finite resonant amplitude and a finite frequency width. We approximated this frequency dependence using the collision broadened profile of Van Vleck and Weisskopf (1945),<sup>10</sup>

$$\bar{W}(\omega) = \frac{\gamma^2 B_{ac}^2}{\hbar^2} |S_{NM}^x|^2 (P_M - P_N) \omega^2 f(\omega, \omega_{NM}), \quad (S3)$$

where  $f(\omega, \omega_{NM})$  takes the form

$$\frac{1}{\pi} \left[ \frac{T_2^{-1}}{(\omega - \omega_{NM})^2 + T_2^{-2}} + \frac{T_2^{-1}}{(\omega + \omega_{NM})^2 + T_2^{-2}} \right].$$

However, we should keep in mind that this EPR line

shape does not account for saturation effects and the associated temperature increment, which for a typical  $ac$  field of 0.1 G occurs for longitudinal relaxation time  $T_1 \gtrsim 1 \mu\text{s}$ .

- 
- <sup>1</sup> J. P. Perdew, K. Burke and M. Ernzerhof, *Physical Review Letters*, 1996, **77**, 3865.
- <sup>2</sup> N. Troullier and J. L. Martins, *Physical Review B*, 1991, **43**, 1993.
- <sup>3</sup> H. Myers and W. Sucksmith, *Proceedings of the Royal Society of London A*, 1951, **207**, 427–446.
- <sup>4</sup> T. Alonso-Lanza, A. Ayuela and F. Aguilera-Granja, *ChemPhysChem*, 2015, **16**, 3700–3710.
- <sup>5</sup> P. Giannozzi, S. Baroni, N. Bonini, M. Calandra, R. Car, C. Cavazzoni, D. Ceresoli, G. L. Chiarotti, M. Cococcioni, I. Dabo, A. Dal Corso, S. de Gironcoli, S. Fabris, G. Fratesi, R. Gebauer, U. Gerstmann, C. Gougoussis, A. Kokalj, M. Lazzeri, L. Martin-Samos, N. Marzari, F. Mauri, R. Mazzarello, S. Paolini, A. Pasquarello, L. Paulatto, C. Sbraccia, S. Scandolo, G. Sclauzero, A. P. Seitsonen, A. Smogunov, P. Umari and R. M. Wentzcovitch, *Journal of Physics: Condensed Matter*, 2009, **21**, 395502–395521.
- <sup>6</sup> G. Kresse and J. Furthmüller, *Physical Review B*, 1996, **54**, 11169–11186.
- <sup>7</sup> G. Kresse and D. Joubert, *Physical Review B*, 1999, **59**, 1758–1775.
- <sup>8</sup> U. von Barth and L. Hedin, *Journal of Physics C: Solid State Physics*, 1972, **5**, 1629.
- <sup>9</sup> A. Kramida, Yu. Ralchenko, J. Reader and NIST ASD Team, NIST Atomic Spectra Database (ver. 5.3), [Online]. Available: <http://physics.nist.gov/asd> [2016, May 6]. National Institute of Standards and Technology, Gaithersburg, MD., 2015.
- <sup>10</sup> A. Abragam and B. Bleaney, *Electron Paramagnetic Resonance of Transition Ions*, Oxford University Press, Oxford, 1970.
- <sup>11</sup> A. Repollés, A. Cornia and F. Luis, *Physical Review B*, 2014, **89**, 054429.
- <sup>12</sup> O. Grinberg and L. J. Berliner, *Very High Frequency (VHF) ESR/EPR*, Springer Science & Business Media, 2013, vol. 22.